

General Overview of the Nature and Use of Satellite Remote Sensing Data for Fisheries Application

J. F. R. Gower

Department of Fisheries and Oceans, Institute of Ocean Sciences
P. O. Box 6000, Sidney, British Columbia, Canada V8L 4B2

Abstract

This paper presents a review of satellite remote-sensing techniques relevant to fisheries science and oceanography. Examples of visible, infrared and microwave images are shown and discussed, and some results from non-imaging sensors are presented. References are given to recent, more detailed reviews and research papers. All of the techniques could have important applications to fisheries science, but few users have sufficient receiving and processing capability to make the fullest use of the data. Although the technology of remote sensing is expanding rapidly, future applications will depend largely on international cooperation in placing new improved sensors in space.

Introduction

This paper presents examples of satellite data which are useful in furthering understanding of the oceans. A full review would need to cover a very wide range of different techniques (e.g., see the special issues of *Oceanus*, Fall 1981), but this overview concentrates on examples that have special relevance to fisheries, particularly to regional studies of productivity and to related ocean dynamics and operational requirements for wind and wave data.

A number of sensing techniques have now been tested from space. The infrared mapping of sea surface temperature patterns is well known and widely used. Ice and cloud cover are monitored at infrared and visible wavelengths. Data collection from buoys or shore stations via satellites also has many applications. Shorter tests have been conducted with satellite-borne radars for wind and wave measurements and for producing high resolution images of ice and water roughness patterns. These techniques, and that of microwave radiometry, demonstrate how a satellite may collect remote-sensing data through clouds during day and night and thus contribute to a regular monitoring or data collection system.

A recent, and still operating, satellite sensor is collecting images showing the changes in water color associated with the chlorophyll pigment concentration in phytoplankton in the sea. Because of the relevance of these data to primary productivity and hence to fisheries, examples of such data will be presented first, followed by measurements of important but less direct relevance.

Satellite Measurements of Water Color

Images from the LANDSAT satellite, such as that in Fig. 1, have been available through NASA (U. S. National Aeronautics and Space Administration) since 1972. The images give 100-m spatial resolution in four spectral bands, two corresponding roughly to green and red light and two in the near infrared at 0.7 to 0.8μ and 0.8 to 1.1μ . Each image covers an area of about $185\text{ km} \times 185\text{ km}$. The sensitivity and digitization levels are set for land targets with relatively high reflectivity, but Fig. 1 shows that water color patterns are sometimes visible in coastal areas, especially where silt-laden river water flows out over the denser sea water to form a spreading plume. In this example, the Fraser River water forms a thin (2-4 m thick) surface layer on the sheltered waters of the Gulf of Georgia. Images such as this have been used to map the extent of the river plume in different wind and tide conditions and hence to study the influence of river water on circulation patterns in fisheries and pollution programs.

The area of the plume is large enough to make aerial mapping difficult but forms a very conveniently-sized target for LANDSAT. The sensitivity of LANDSAT, however, does not allow mapping of the more subtle color changes farther from the river mouth, and the long coverage cycle of the satellite (an orbital path is repeated every 18 days) makes cloud-free observations very infrequent. The size of an individual scene is also very small compared to an ocean basin. These disadvantages have greatly restricted the use of LANDSAT data for oceanographic purposes.

On some occasions, even sporadic satellite coverage will detect unusually bright water color patterns



Fig. 1. LANDSAT Multi-spectral Scanner image taken in the red region of the visible spectrum (600–700 nm) showing the Vancouver-Victoria area of British Columbia, Canada on 30 July 1972. (The plume of silty water from the Fraser River is clearly visible in the center of the scene; there is a cloud over the Strait of Georgia in the top left; some thin haze patterns, e.g. over Juan de Fuca Strait near the bottom, are difficult to distinguish from water color changes in a single band image such as this.)

offshore, caused by strong plankton blooms in highly productive conditions. An example of such a pattern is shown in Fig. 2. This is a green-band LANDSAT image taken south of Iceland in the North Atlantic on 19 June 1976. The scene, 185 km across as before, shows part of what is evidently a much more extended plankton bloom, in which water with higher surface concentrations of light-scattering phytoplankton returns more light to the satellite's optical sensor. The pattern is caused by advection of the water in mesoscale turbulent motion, and the average spatial structure of this turbulence can therefore be deduced from such an image (Gower *et al.*, 1980). The characteristic time scale of such a bloom is a few days, and no other image of this event was recorded by the satellite.

Clearly, one can imagine a satellite sensor better designed to map such transient phenomena. A wider angle of view means that areas are covered more often, even on days when the satellite does not pass directly overhead. Greater sensitivity can allow faint water color changes to be detected, although the light back-scattered by the atmosphere gives a high background to be subtracted. Choice of wavelength bands allows the characteristic water color variations to be selectively extracted from the data.

A sensor designed to map water color, the Coastal Zone Color Scanner on NIMBUS-7, has been in orbit since 1978. It has demonstrated that color patterns can be detected over large areas of the ocean and that the



Fig. 2. Enhanced LANDSAT image in the green band (400-500 nm) showing increased water reflectance in the Atlantic Ocean south of Iceland on 19 June 1976. (The patterns are interpreted as being due to a plankton bloom in water advected by mesoscale turbulence; haze patterns have been reduced using image data in the longer wave-bands but some dark and light streaks remain.)

mean surface chlorophyll concentration responsible for the color changes can be calculated (Hovis *et al.*, 1980; Gordon *et al.*, 1980).

The chlorophyll is present in the phytoplankton which forms the first stage of biological productivity of the sea. Mapping of the patterns of primary productivity and studying their long and short-term variations

are basic tasks of ocean ecology. Movement of any color patterns visible to a satellite can also be used in following ocean currents and in tracing the mixing and upwelling that bring the nutrients needed for this productivity. To some extent, the usual disadvantage of the satellite, in being restricted to viewing only the ocean surface, is here less important because photosynthesis, and hence phytoplankton growth, is similarly restricted to the sunlit near-surface layer. Subsurface maxima of phytoplankton concentration that tend to be formed in highly stratified water, however, will only be imperfectly sensed from space.

Figure 3 shows an example of a Coastal Zone Color Scanner image. The data are collected in four high-sensitivity bands of visible light, each 20 nm wide in the blue, blue-green, green and red regions of the spectrum (443, 520, 550 and 670 nm). The blue band is at a wavelength where light is strongly absorbed by chlorophyll pigments present in phytoplankton, whereas the dominant effect in the green band is back-scattering by other cellular material in the plankton. The presence of pigment will therefore be indicated by a decrease in blue radiance, with a corresponding increase in the green.

This change of sea color, from blue to lighter green with increasing phytoplankton content, has been familiar to sailors and fishermen for centuries, and has been used for navigation and for locating productive

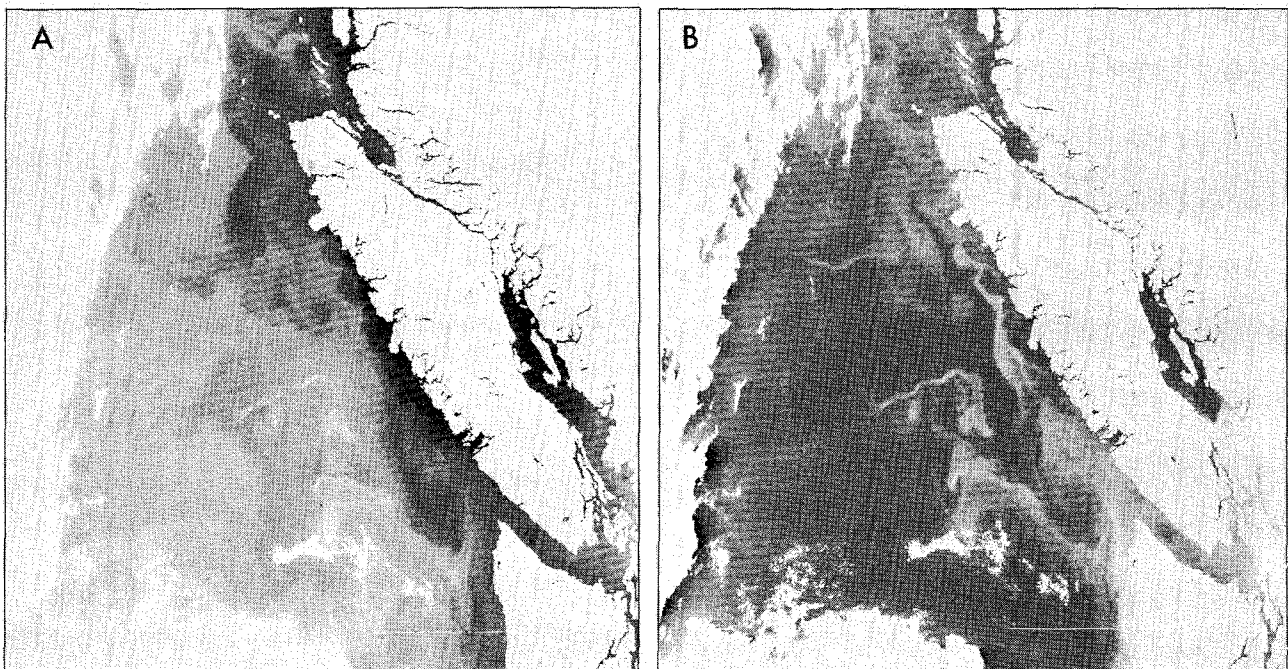


Fig. 3. Coastal Zone Color Scanner image of a cloud-free area west of Vancouver Island, Canada, on 14 July 1979, showing (A) blue-band scene of water color patterns where increasing phytoplankton content leads to less brightness because of high absorption by chlorophyll pigments, and (B) green-band scene of patterns where increasing phytoplankton content leads to more brightness because of back-scattering from other cellular material in the plankton.

areas. The Coastal Zone Color Scanner has shown that these color changes can be measured from space and hence monitored regularly over large areas. To do this accurately, the effect of the atmosphere must be allowed for. The contribution of Rayleigh scattering from atmospheric gases can be calculated, and much of the effect of haze and thin cloud can be deduced from measurements in the red band. At the longer wavelengths of this band, increasing absorption by the sea water itself reduces radiance back-scattered from below the surface, and most of the observed radiance is returned by back-scattering in the atmosphere. Especially over relatively clear water, therefore, the radiance in this channel is a measure of the atmospheric contribution alone and can be used to deduce corrections to the data collected by the other three channels. For more turbid water, some water radiance is still present, and a longer wavelength (infrared) channel would be needed to give a nearly black background for measurement of the atmospheric signal.

Blue and green band images of a cloud-free area off the west coast of Vancouver Island on 14 July 1979 are shown in Fig. 3A and 3B respectively. These have both been corrected for Rayleigh scattered light and for the effects of thin haze. The eddy near the center of the image shows the relative darkness in the blue and brightness in the green wavelengths, characteristic of increased phytoplankton concentration. Several other areas, including a hammerhead feature farther southward, behave similarly. In Fig. 4, the ratio of these two images is formed to emphasize such areas. Increased

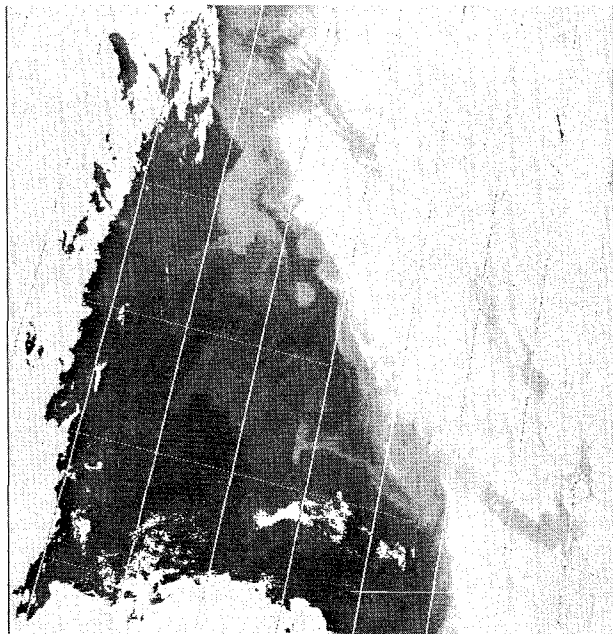


Fig. 4. The green to blue ratio image formed by dividing the pixel values of Fig. 3B by those of Fig. 3A, showing brightness levels related to chlorophyll concentrations noted in the text.

brightness in the green to blue ratio image may then be interpreted as indicating increased chlorophyll. Bright areas in both bands are interpreted as containing more scatterers but relatively less pigment. Dark areas in both bands are again interpreted according to the value of the ratio, although dissolved organic matter in the fresh water runoff may also be increasing the ratio in the area close to the coast.

A large amount of ocean optics data has now been collected with a view to deriving a quantitative relation between this green to blue ratio and the near-surface chlorophyll concentration. The general conclusion has been that, in water where optical properties are dominated by the presence of phytoplankton, the average spectrum of light from the water is related to the chlorophyll pigment concentration and the diffuse attenuation coefficient as shown in Fig. 5 (Austin and Petzold, 1981). At low pigment concentrations ($<0.1 \text{ mg/m}^3$), a considerable amount of blue light is scattered back upwards. Up to about 0.7 mg/m^3 , the blue light diminishes, and the reflection of green light increases at higher levels. The curves in Fig. 5 are

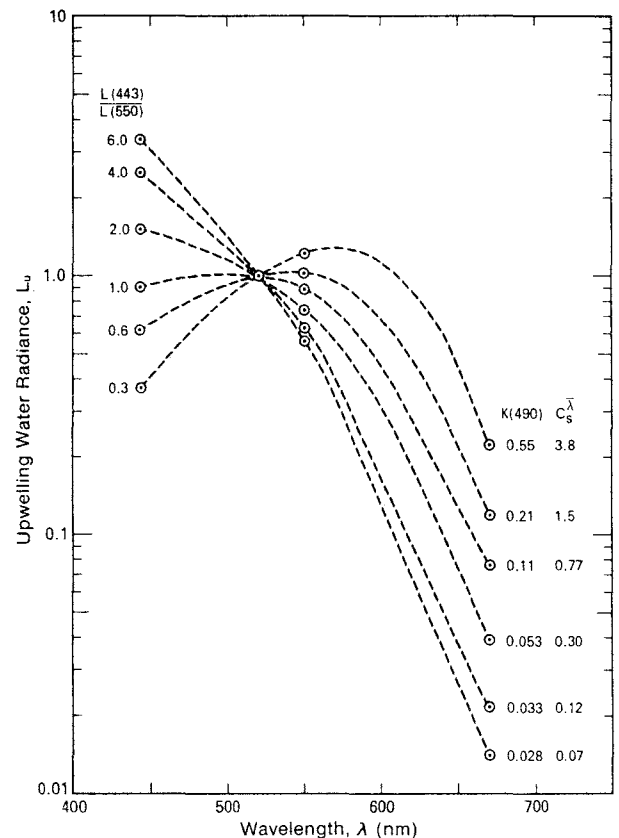


Fig. 5. Upwelling radiance spectra for sunlight illumination of sea-water whose optical properties are dominated by the presence of phytoplankton (from Austin and Petzold, 1981). (These curves represent a best fit model to many observations from locations around the world and are used to interpret the satellite images shown in Fig. 3 and 4.)

normalized at 520 nm (blue/green) to remove some of the variation due to broad-band back-scatter. These curves show the water spectral variation that is mapped in the ratio image (Fig. 4). Water affected by coastal sediment or dissolved organic matter will not behave in the same way, making quantitative determination of chlorophyll more difficult. Use of the data in Fig. 5 to interpret the patterns in Fig. 4 indicates that waters in the eddy and the hammerhead feature contain about 2 mg/m^3 of chlorophyll pigment, with higher values of 5 mg/m^3 near shore and lower values ($<0.5 \text{ mg/m}^3$) farther offshore.

Apart from giving quantitative results of this kind, features visible in Fig. 3 and 4 suggest a variety of water movements. These include a flow of more productive water out of Hecate Strait southward around the northern tip of Vancouver Island and a band of less productive water moving northwestward close to the west coast of Vancouver Island. Eddies at the edge of this northwestward flow are visible in the more productive water against the coast. Water movement out of Juan de Fuca Strait (south of Vancouver Island) is also suggested by the counter-clockwise eddy of productive water near its mouth and by the hammerhead feature farther offshore. A thermal infrared image of the same region (Fig. 6), taken by the NOAA-5 AVHRR Scanner 2.5 hours after that shown in Fig. 4, shows temperature contrasts due to tidal mixing in inshore waters but very few of the offshore features that are visible in the color data. Water color images can thus give quantitative data as well as maps of contrasts and boundaries in a manner analogous to thermal infrared images. The above discussion also indicates that the color data can show structures not previously visible from space.

A large quantity of NIMBUS-7 water color data has now been collected covering many parts of the world. Figure 7 is an example of chlorophyll pigment and diffuse attenuation coefficient images for waters off eastern Canada and northeastern United States on 14 June 1979. Atmospheric corrections, followed by fitting of the data to the water radiance spectra illustrated in Fig. 5, lead to numerical values given against the step-wedge beneath the two images. Georges Bank (east and southeast of Cape Cod) and inshore Gulf of Maine waters are shown as the most productive areas with lesser pigment values associated with the Scotian Shelf. Low pigment values occur in the Gulf Stream at the bottom edge of the image, where the northern tip of a warm-core eddy can just be seen.

Several new sensors are being planned for research of the type described above, among them the DFO (Canada) Fluorescence Line Imager (Gower, 1982). This device will make use of solid state imaging techniques to allow measurement of the natural fluorescence signal from chlorophyll a (Gower and Bor-

stad, 1981) as well as to improve the sensitivity of measurements, such as those given above, based on absorption. Mapping two properties of the chlorophyll a simultaneously should lead to increased accuracy in the results and may also allow changing properties of the phytoplankton to be studied as it grows and decays.

NASA's Coastal Zone Color Scanner is still in orbit, but it is failing fast, and color sensors planned for

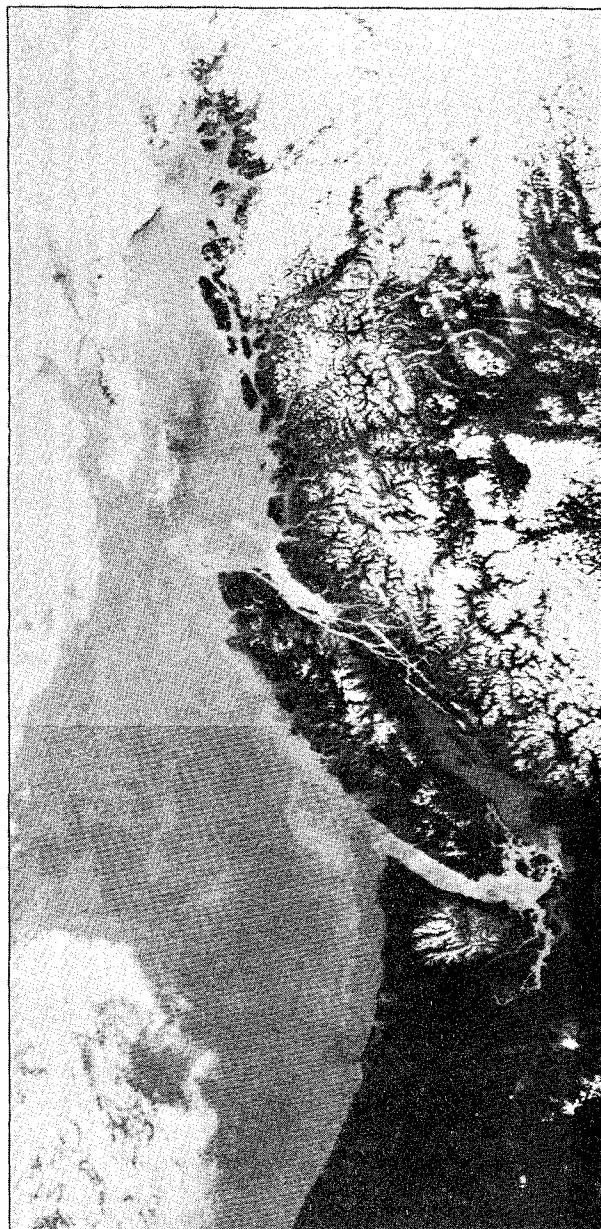


Fig. 6. Thermal infrared imagery from the NOAA-5 AVHRR sensor showing Vancouver Island and vicinity taken at 2234 hr GMT on 14 July 1978, or 2.5 hours after the images in Fig. 3 and 4. (Effects of tidal mixing in inshore channels show strongly but few of the offshore patterns are seen.)

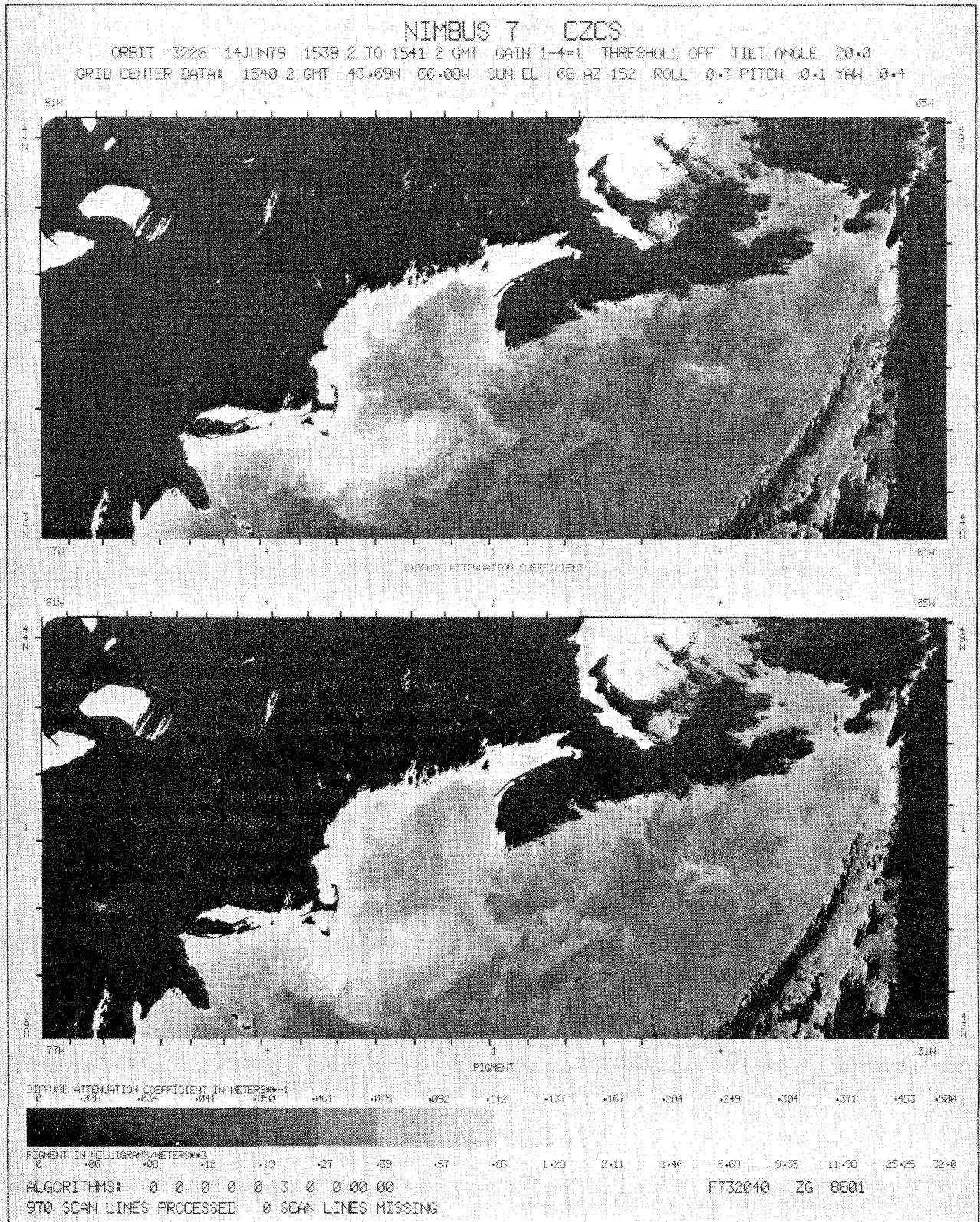


Fig. 7. Coastal Zone Color Scanner images taken on 14 June 1979, showing diffuse attenuation coefficient (upper) and chlorophyll pigment (lower) for the coastal regions of eastern Canada and United States. Values for both parameters are given against the step wedge at the bottom. (Higher phytoplankton concentration on Georges Bank and in coastal areas can be clearly seen.)

NOSS and for the European ERS-1 satellites have been cancelled. The color data have valuable applications in a number of fields and NASA is presently searching for opportunities to launch a second sensor, with minor improvements, in the near future.

Thermal Infrared Mapping

Infrared images showing sea-surface temperature contrasts have been available for about 10 years. The data have been used both for temperature determination and for mapping structure and movements of surface water. Such data are collected routinely by weather satellites for cloud imaging but are less often available in the enhanced form suitable for mapping sea-surface temperatures.

An example of an enhanced infrared image is shown in Fig. 8. The thermal contrast between warm Gulf Stream water and cooler shelf water shows up strongly. Processes that mix the two, such as large-scale instabilities and eddy formation and their effect on the movement of shelf water, can be studied from such images, as discussed by Chamberlin (1982). The coverage is, however, strongly limited by cloud, and images showing features east of 60°W are quite rare. This is unfortunate because the dynamics around the

southern Grand Bank are particularly important for studying shelf water exchange on the bank, and the interaction of the Labrador Current and Gulf Stream forms strong dynamic patterns near Flemish Cap. In fact, there is a general tendency for strong thermal contrast on the sea surface to cause cloud formation, so that many interesting areas around the world will be screened from satellites.

The limitation is equally strong for visible as for infrared radiation. Cloud penetration requires observation at micro-wavelengths using active (radar) or passive (radiometric) techniques. At these wavelengths, no "color" effects remain because microwave quanta are far too weak to stimulate biochemical reaction. Thermal effects can be detected, but surface reflectance variations are usually the dominating influence on the sensor signal.

Synthetic Aperture Radar Imagery

Images of surface microwave reflectance variation can be formed with extremely high spatial resolution using synthetic aperture (side-looking) radar (SAR). Received signals at successive locations along the satellite's orbit are combined to give a resolution (for SEASAT) of 25 m. This requires combining signals



Fig. 8. Infrared image taken on 28 April 1974, showing structures associated with the north wall of the Gulf Stream south of Cape Cod and Nova Scotia in the Northwest Atlantic. (Warm core eddies form and move westward in the edge of the colder shelf water.)

received over a time of about 2 sec, during which the satellite's motion traces out a "synthetic aperture" antenna about 15 km long. The synthesis involved in forming the image is complicated and time consuming for even a specially configured computer. The process assumes that the targets are stationary during the 2-sec period, and motions or changes, such as those due to surface wave motion, can lead to blurring, shifting and lack of contrast in the final image. The radar return is preferentially from short waves satisfying the Bragg condition and so having roughly the same wavelength as the radar. These waves will form mean roughness patterns that are anisotropic, being caused by wind or longer waves moving in a particular direction. The visibility of surface patterns to a SAR can therefore change, but, in general, roughness variations, due to surface or internal wave motion, wave refraction at current boundaries, wind variation, or atmospheric boundary-layer stability changes, can be imaged with high geometric precision. Several examples exist where the SAR imagery shows effects of currents flowing over varying bottom topography, or the results of shear patterns in the Gulf Stream (Hayes, 1981) or in warm-core eddies (Lichy *et al.*, 1981).

The more obvious changes due to sea ice or coastline will generally show clearly, but the contrast is not fixed because the mean roughness of the sea varies with wind speed. Figure 9 is an example of a SEASAT SAR image, in which smooth shorefast ice and offshore floes give low radar return and appear dark, the rougher shore lead appears grey, and rougher areas in the ice pack farther offshore give greater radar return and appear brighter. A different choice of radar incidence angle can improve the ice-water contrast situation in future systems, and SAR can certainly be usefully applied to mapping sea ice.

Because of the high spatial resolution achieved, SEASAT SAR images show surface wave patterns down to wavelengths of 50–100 m, whose mean length and direction agree well with surface observations (Gonzales *et al.*, 1981; Vesecky *et al.*, 1981). In fact, because surface observations are limited by the inher-

ent randomness of the wave field, averaging over an area of a satellite image might be expected to give a superior indication of these two parameters, although direction can only be deduced with a two-fold ambiguity since the image only shows wave "crest" lines. An example of such an image (Fig. 10) shows surface waves travelling from the west (left to right) and being diffracted around Sumburgh Head at the southern tip of the Shetland Islands northeast of Scotland. The ocean waves here have a mean wavelength of 200 m, well within the capability of a radar having 25 m resolution. In this rather special case, the diffraction solves the direction ambiguity problem.

Other information on the wave spectrum can be deduced from such images. To some extent the lengths of the crest lines indicate the angular width in the wave spectrum. A spatial frequency analysis (two-dimensional Fourier transform) can show several wavelength components, possibly moving in different directions. The complete wave spectrum would only be produced if the radar image brightness were linearly related to sea-surface height at each point. Since the relation should involve slope, surface convergence and motion, a full simple answer cannot be expected. Comparisons show, however, that the peak wave components are accurately mapped, but with a variable lower limit of wave height which depends on the direction from which the radar views them. Detection of shorter waves depends critically on maintaining the full spatial resolution of the radar through precise processing.

Other roughness patterns caused by ocean dynamics or boundary-layer effects are visible in SAR images, especially at low wind speed. Internal waves, fronts and eddies, rain cells and surface wind patterns have all been mapped. A volume edited by Beal *et al.* (1981) provides a good review of the use of SAR for oceanography, with examples.

The combination of available satellite power, data band width and processing throughout limits the coverage of SAR imagery. SEASAT gave narrow swaths in

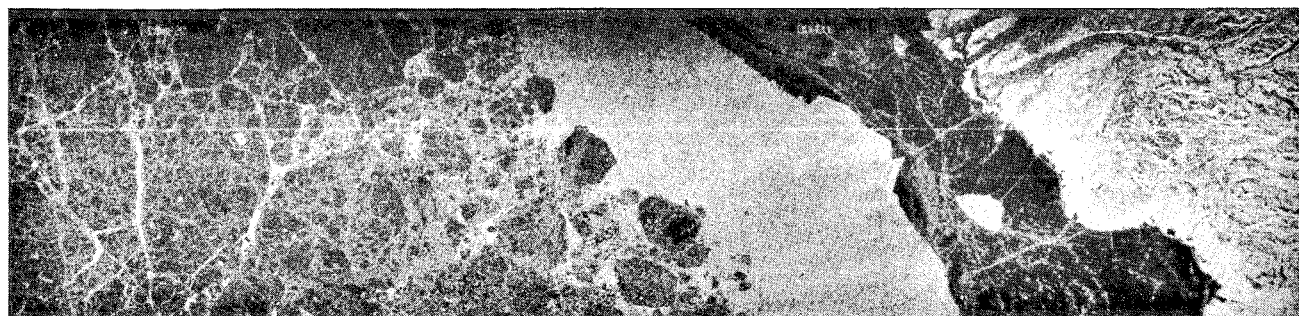


Fig. 9. Optically-processed SEASAT SAR image of an area 18 by 75 miles in the Beaufort Sea, showing from left to right (west to east) sea ice floes, open water, shorefast ice and the coast of Banks Island, Canada.

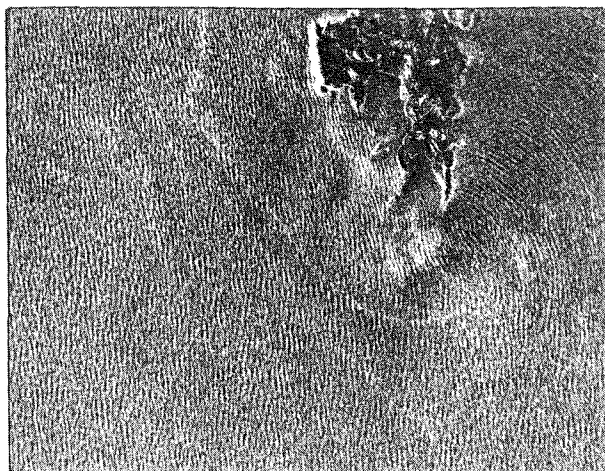


Fig. 10. Digitally-processed SEASAT SAR image taken on 15 September 1978, showing ocean waves of 205 m wavelength moving from west to east (left to right) and diffracting around Sumburgh Head at the southern tip of the Shetland Islands, northeast of Scotland.

a pattern that would take roughly 25 days for full earth coverage. Separated swaths of wave data from such a pattern could be used as input to a directional spectral wave model, but a map of surface wind velocity would be more useful for input to an operational wave model. The scatterometer on SEASAT was designed to provide such wind data.

Scatterometer Measurements of Wind Speed

A scatterometer measures the directional properties of the microwave reflectivity caused by wind-induced roughness of the sea surface (Jones *et al.*, 1981). This roughness is anisotropic in the sense that, for oblique viewing, the measured cross-wind microwave reflectivity is less than that in the upwind or downwind direction. The SEASAT scatterometer measured reflectivity of elements of the sea surface in two azimuths at right angles, using four beams each with incidence angles of 20° to 50° . Use of Doppler information provided a spatial resolution of 50 km over a swath 500 km wide, beginning 200 km from nadir, on each side of the spacecraft. If both measured reflectivities are equal, the wind direction must be between the two azimuths of measurement or at right angles to this, leading to a fourfold (90°) ambiguity. If the two reflectivities differ by the maximum value expected from measurements of the anisotropy, the wind direction is identified with only twofold (180°) ambiguity because the direction with higher reflectivity must be upwind or downwind. In the more general case, a smaller measured difference leads to a fourfold ambiguity of direction, two 180° ambiguities separated by an acute angle.

The instrument met its goal of providing wind speeds within ± 2 m/sec or 10% of surface measurements, and directions within $\pm 20^\circ$ when some external means of ambiguity removal was used. The scatterometer has the advantage of providing a spatially averaged measurement, so avoiding problems with random fluctuations in the wind field. Also, the surface reflectivity may be providing a better measurement of surface wind stress, as needed for wave forecasting, than of wind speed, but this has not been tested directly.

Figure 11 is an example of scatterometer data plotted to show patterns of surface wind. Numbers give the measured speed, and short lines indicate possible directions with twofold or fourfold ambiguity. Studies of data (NASA, 1980) show that patterns of cyclones, anticyclones and cols can be identified and plotted in spite of the ambiguities without making use of any other information. The resulting locations are superior to those deduced from satellite cloud images in which high level cloud can obscure surface features. Scatterometer coverage is much denser than that from conventional ship observations, and frequent examples have been found where scatterometer data would have improved standard analyses.

Scatterometer data from a single satellite could provide sufficient wind data input for a suitably designed directional wave model. An improved instrument of the SEASAT type was planned for NOSS, but this program has been cancelled and future work must await European or Japanese developments.

Microwave Radiometry

The ocean emits thermal energy in the microwave region of the spectrum as well as in the infrared. Because such energy is relatively unaffected by clouds, all weather sea-surface temperature mapping is possible (Hofer *et al.*, 1981; Njoku and Hofer, 1981). The signal is affected by surface and atmospheric conditions, most importantly roughness and cloud water content, but the instruments on SEASAT and NIMBUS-7 satellites demonstrated that a multichannel scanning radiometer can separate out the confusing effects into separate maps of water temperature, surface wind speed, atmospheric water vapor and cloud water content (Njoku and Hofer, 1981; Chang *et al.*, 1981). Over ice, a similar separation into the fractional cover of multi-year and first year ice also seems possible (Gloersen *et al.*, 1981). The spatial resolution of such maps will be low, depending on the lowest microwave frequency needed. In the calculations for water temperature, the SEASAT and NIMBUS-7 instruments observing at 6.6 GHz averaged over 130 km. A much

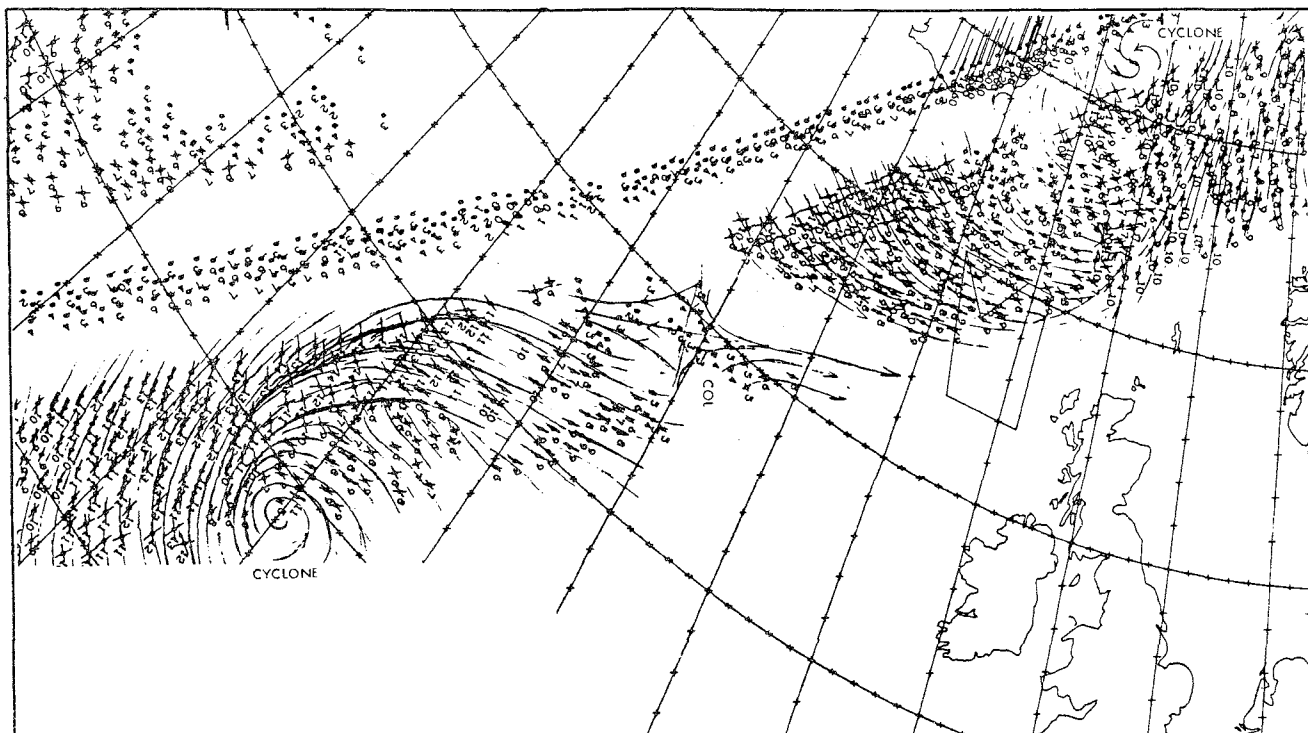


Fig. 11. Scatterometer wind vectors, with two- and four-fold ambiguities, as observed over the North Atlantic on 22 August 1978. (These are interpreted as a cyclone-col-cyclone pattern.)

larger antenna (4 m) was planned for NOSS which would have reduced this to about 35 km.

Under moderate weather conditions, the passive microwave sensor can measure temperature to about the same accuracy as infrared sensors but with the great advantage of cloud penetration. The measurements are strongly affected by sun glint and man-made interference, both of which limits their usefulness in an operational system. Wind measurements, giving speed only, are about as accurate as those from the scatterometer.

The information provided by the radiometer on atmospheric properties, particularly water content, is useful in correcting for absorption of scatterometer signals and for delay of the altimeter pulses. Radiometers may therefore be included in an auxiliary role for this purpose. Figure 12 gives the results calculated from SEASAT radiometer data as the satellite passed over Hurricane Fico in the Pacific Ocean on 20 July 1978. The winds calculated from the radiometer are here compared with those derived from scatterometer data. They agree well except near the center of the hurricane. The radiometer shows high water content, whose attenuation would be expected to reduce the scatterometer return signal and lead to erroneously low results if uncorrected. The surface temperatures indicated here may also be affected by water vapor content of the atmosphere; the algorithms are still being refined.

Salinity changes of 0.2 to 1 part per thousand can also be sensed by low frequency radiometers operating below a frequency of 2 GHz. However, the problems of low spatial resolution become more extreme than for temperature, although it is possible that a large microwave dish, about 100 m in diameter, could map surface salinities on a 2 km scale sometime in the future. At present, there are no plans to put such an instrument into space, although much smaller airborne sensors have demonstrated the principle (Kendall and Blanton, 1981).

Altimeter Measurements of the Sea Surface

An altimeter measures the total travel time for a microwave pulse transmitted downward and reflected back to the satellite from the ocean surface directly beneath. Since this pulse width can be equivalent to about 0.5 m of range difference, its shape will be strongly distorted by reflection from points at different heights on the sea surface (Townsend *et al.*, 1981). This pulse shape is recorded and used to give a direct measurement of the distribution of surface height, for which the significant waveheight ($H_{1/3}$) can be computed. The distribution is measured over a circular area, centered on the nadir, of radius 1.2 to 6 km depending on the waveheight. The spatial averaging reduces the effect of random fluctuations in the wave field to roughly the same extent as the 20 min of temporal averaging common in analyzing waverider

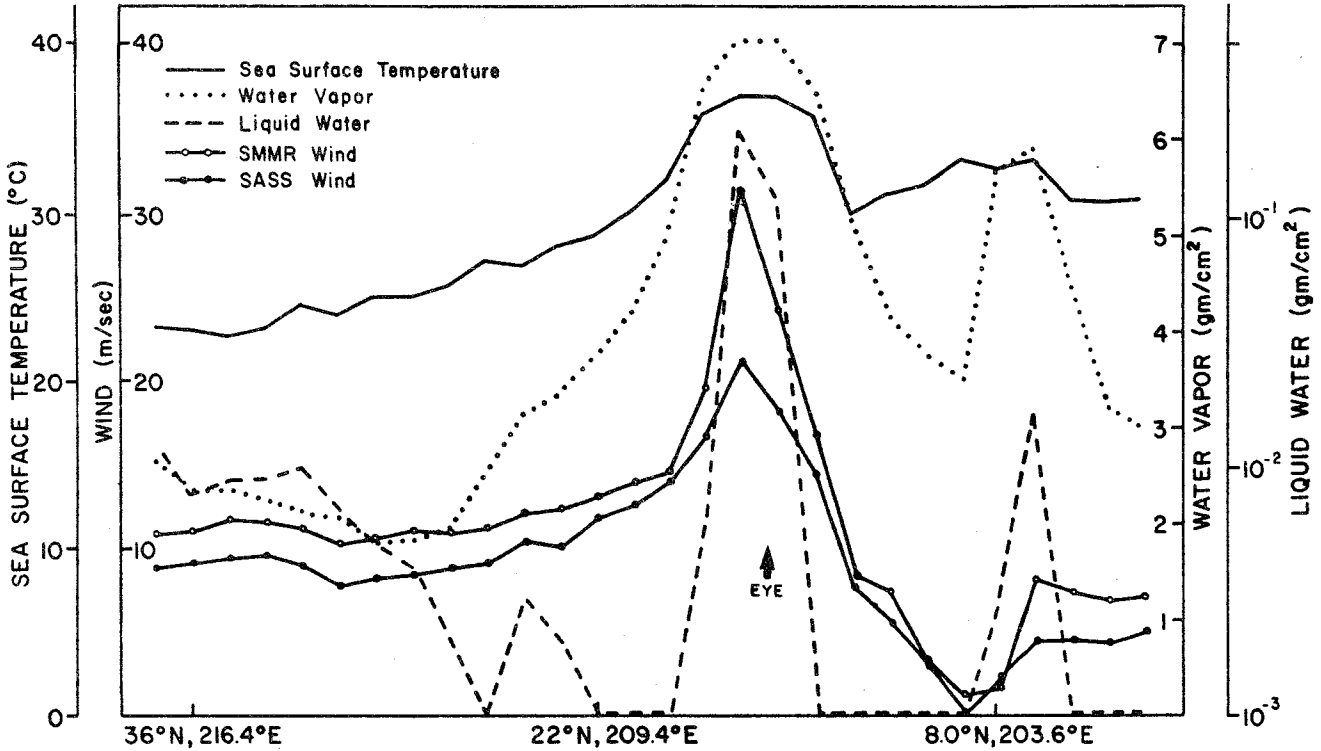


Fig. 12. Profiles of sea-surface temperature, surface wind speed, total atmospheric water vapor and liquid water content, calculated from SEASAT radiometer (SMMR) data as the satellite passed over Hurricane Fico in the Pacific Ocean on 20 July 1978. (The comparison with scatterometer wind measurements shows the advantage of radiometer data in allowing correction for atmospheric effects.)

records. Further spatial averaging is possible as the satellite proceeds along its track.

The SEASAT altimeter gave waveheight measurements to ± 0.5 m or to 10% (whichever was larger), but estimates of its accuracy are largely limited by the accuracy of data from conventional buoys and ships. These waveheight data are only available for points directly beneath the satellite, so that coverage in one day is along the lines of a very coarse grid with spacings of about 3,000 km. The coverage still provides a large amount of wave data of higher quality than those provided by standard ship reports, and would be a valuable contribution to wave modelling and forecasting.

The altimeter's range measurements, when corrected for the satellite's orbital positions and the precise shape of the local geoid, show mean sea-surface height variations related to major ocean current systems, such as the Gulf Stream. The geostrophic balance of an ocean current on a rotating earth implies a slope of the sea surface proportional to the water speed. At the northwest wall of the Gulf Stream, there is a 1-m height change over several kilometers. Comparisons of surface height and wave height measurements (Townsend *et al.*, 1981) show cases in which the waveheights appear strongly related to the current, presumably due to wave-current interaction (Fig. 13). Such an

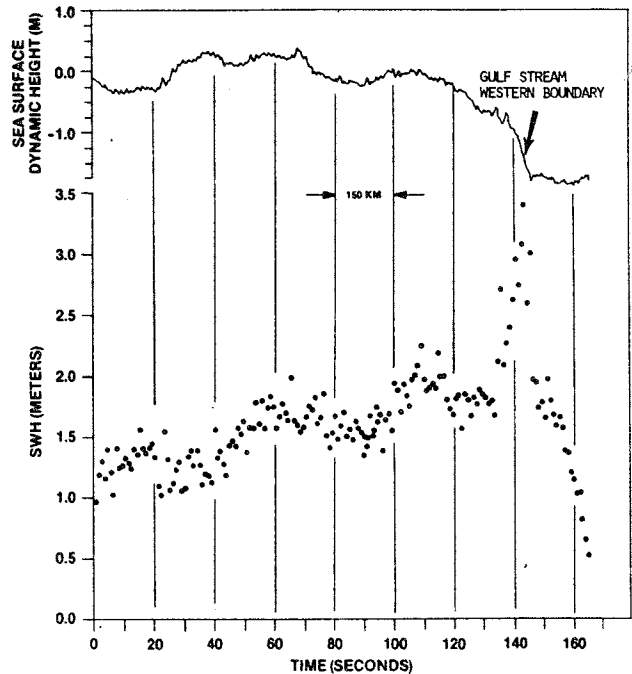


Fig. 13. Sea-surface dynamic heights and significant wave heights calculated from SEASAT altimeter data collected on 28 September 1978.

effect is a well known, but poorly defined, hazard for ocean operations.

Other features of the sea-surface height profile, measured by an altimeter beneath the satellite, can be related to the vertically integrated motion in eddies (Cheney and Marsh, 1981). Figure 14 shows examples of altimeter measurements over a repeated track as a cold eddy drifts slowly past. Passage of an eddy would be seen even if the eddy were capped with warmer Sargasso Sea water.

The precision of satellite altimeters has progressed from about 25 cm for GEOS-3 to about 5 cm for SEASAT. The NOSS instrument would have been similar to that of SEASAT, but a major new project planned to measure circulation of the world's oceans (Topex) would aim for an accuracy of 2 cm. The Gulf Stream slope was detected by the GEOS-3 satellite and accurately measured by SEASAT. The return flows in the eastern Atlantic, however, give very much smaller slopes and make the high precision of Topex necessary. Such precision can only be achieved by careful attention to satellite tracking in a specially-selected stable orbit, to gravity determinations using an associated Gravsat experiment, and to correction for atmospheric loading and propagation delay. Scatterometer measurements at the same time are also

required so that the current measurements can be interpreted in terms of wind forcing.

The total project is a major one that would significantly improve the knowledge of ocean dynamics. The proposed period is 5 years, during which variability could be related to observed changes in fisheries, for example. Such a project would also provide new information on ocean heat budgets for studying climatic changes on longer time scales.

General Conclusions

The above survey discusses a variety of remote-sensing data from the biologically related color measurements to large-scale general circulation studies. All could have important applications to fisheries science, but all are in a more or less developmental phase and, in some cases, the necessary satellite sensor is not yet in orbit. However, the potential of satellites has been demonstrated.

Full realization of the potential takes time. After a sensing technique has been tested and found useful, there will be several years before it is in widespread use, even for the direct and graphic example of thermal infrared imagery. Surface temperature data have been available from weather satellites for more than 10 years, but few users have sufficient (or sufficiently cheap) receiving and computing capability to make the fullest use of the data. This only comes with the ability to store large amounts of data, apply corrections, transform the data to a common geometrical grid, and then map trends and movements. The data-collecting capabilities of satellite remote sensing make necessary an improvement and cheapening of processing equipment equivalent to one or perhaps two "generations" of new development. This technology is expanding rapidly and the use of satellite data can therefore become much more widespread in the future. The major uncertainty at present is in funding for the launch of new satellites. International cooperation here, as in other areas, is essential.

References

- AUSTIN, R. W., and T. J. PETZOLD. 1981. The determination of the diffuse attenuation coefficient of sea water using the Coastal Zone Color Scanner. *In* Oceanography from Space, J. F. R. Gower (ed.), Plenum Press, New York, p. 239-256.
- BEAL, R. C., P. S. de LEONIBUS, and I. KATZ. 1981. Spaceborne synthetic aperture radar for oceanography. John Hopkins Univ. Press, Baltimore, 215 p.
- CHANG, A. T. C., T. T. WILHEIT, and P. GLOERSEN. 1981. Global maps of atmospheric water vapor, cloud water and rainfall derived from NIMBUS-7 Scanning Multichannel Microwave Radiometer data: a case study. *In* Oceanography from space, J. F. R. Gower (ed.), Plenum Press, New York, p. 683-689.

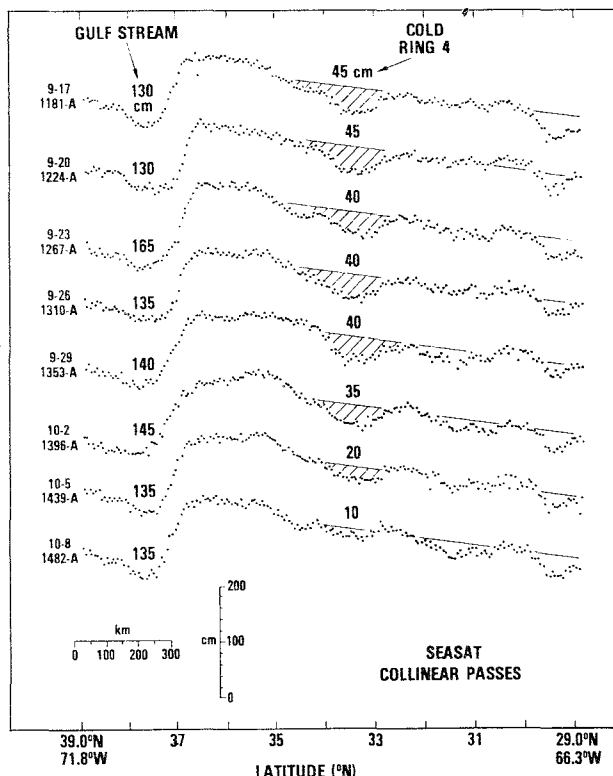


Fig. 14. Sea-surface dynamic heights calculated from altimeter data at 3-day intervals from eight passes of SEASAT over the same track across the Sargasso Sea and Gulf Stream from southeast to northwest. (The passes show a cold ring causing an initial 45 cm depression (top) which becomes less as the ring moves away from the satellite's track.)

- CHAMBERLIN, J. L. 1982. Application of satellite infrared data to analysis of ocean frontal movements and water mass interactions off northeastern United States. *NAFO Sci. Coun. Studies*, this volume, p. 21-30.
- CHENEY, R. E., and J. G. MARSH. 1981. SEASAT altimeter observations of dynamic topography in the Gulf Stream region. *J. Geophys. Res.*, **86**: 473-483.
- GLOERSEN, P., W. J. CAMPBELL, and D. CAVALIER. 1981. Global maps of sea ice concentration, age and surface temperature derived from NIMBUS-7 Scanning Multichannel Microwave Radiometer data: a case study. *In Oceanography from space*, J. F. R. Gower (ed.), Plenum Press, New York, p. 777-783.
- GONZALES, F. I., R. A. SCHUCHMAN, D. B. ROSS, C. L. RUFENACH, and J. F. R. GOWER. 1981. Synthetic aperture radar observations during GOASEX. *In Oceanography from space*, J. F. R. Gower (ed.), Plenum Press, New York, p. 459-467.
- GORDON, H. R., D. K. CLARK, J. L. MUELLER, and W. A. HOVIS. 1980. Phytoplankton pigments from the NIMBUS-7 Coastal Zone Color Scanner's comparisons with surface measurements. *Science*, **210**: 63-66.
- GOWER, J. F. R. 1982. The "Fluorescence Line Imager" program for improved mapping of sea-surface chlorophyll from space. *NAFO Sci. Coun. Studies*, this volume, p. 61-62.
- GOWER, J. F. R., and G. BORSTAD. 1981. Use of the *in vivo* fluorescence line at 685 nm for remote sensing surveys of surface chlorophyll *a*. *In Oceanography from space*, J. F. R. Gower (ed.), Plenum Press, New York, p. 329-338.
- GOWER, J. F. R., K. L. DENMAN, and R. T. HOLYER. 1980. Phytoplankton patchiness indicates the fluctuation spectrum of mesoscale oceanic structure. *Nature*, **288**: 157-159.
- HAYES, R. M. 1981. Detection of the Gulf Stream. *In Spaceborne synthetic aperture radar for oceanography*, R. C. Beal, P. de Leonibus and I. Katz (eds.), John Hopkins Univ. Press, Baltimore, p. 146-160.
- HOFER, R. E. G. NJOKU, and T. W. WATERS. 1981. Microwave radiometric measurements of sea surface temperature from the SEASAT satellite: first results. *Science*, **212**: 1385-1387.
- HOVIS, W. A., D. K. CLARK, F. ANDERSON, R. W. AUSTIN, W. H. WILSON, E. T. BAKER, D. BALL, H. R. GORDON, J. L. MUELLER, S. Z. EL-SAYAD, B. STURM, R. C. WRIGLEY, and C. S. YENTSCH. 1980. NIMBUS-7 Coastal Zone Color Scanner: system description and initial imagery. *Science*, **210**: 60-63.
- JONES, W. L., F. J. WENTZ, and L. C. SCHROEDER. 1981. Microwave scatterometer measurements of oceanic wind vector. *In Oceanography from space*, J. F. R. Gower (ed.), Plenum Press, New York, p. 553-562.
- KENDALL, B. M., and J. O. BLANTON, 1981. Microwave radiometer measurement of tidally induced salinity changes off the Georgia coast. *J. Geophys. Res.*, **86**: 6435-6441.
- LICHY, D. E., M. G. MATTIE, and L. J. MANCINI. 1981. Tracking of a warm water ring. *In Spaceborne synthetic aperture radar for oceanography*, R. C. Beal, P. de Leonibus and I. Katz (eds.), John Hopkins Univ. Press, Baltimore, p. 171-182.
- NASA. 1980. SEASAT-JASIN workshop report, Vol. 1. Jet Propulsion Laboratory, California Institute of Technology, Pasadena, Calif., Publication 80-62, 397 p.
- NJOKU, E. G., and R. HOFER. 1981. SEASAT SMMR observations on ocean surface temperature and wind speed in the North Pacific. *In Oceanography from space*, J. F. R. Gower (ed.), Plenum Press, New York, p. 673-681.
- TOWNSEND, W. F., J. T. McGOOGAN, and E. J. WALSH. 1981. Satellite radar altimeters: present and future oceanographic capabilities. *In Oceanography from space*, J. F. R. Gower (ed.), Plenum Press, New York, p. 625-636.
- VESECKY, J. F., M. M. ASSAL, and R. H. STEWART. 1981. Remote sensing of the ocean waveheight spectrum using synthetic aperture radar images. *In Oceanography from space*, J. F. R. Gower (ed.), Plenum Press, New York, p. 449-457.
-

